

Electronic Supplementary Information (ESI)

Polymer nanocomposites from free-standing, macroscopic boron nitride nanotube assemblies

Keun Su Kim,^a Michael B. Jakubinek,^a Yadienka Martinez-Rubi,^a Behnam Ashrafi,^b Jingwen Guan,^a Kayla O'Neill,^b Mark Plunkett,^a Amy Hrdina,^a Shuqiong Lin,^a Stéphane Dénomée,^a Christopher T. Kingston^a and Benoit Simard^{*a}

^a Security and Disruptive Technologies Portfolio, National Research Council Canada, 100 Sussex Dr., Ottawa, Canada

^b Aerospace Portfolio, National Research Council Canada, 5145 Decelles Av., Montreal, Canada

*Corresponding Author: Benoit.Simard@nrc-cnrc.gc.ca

BNNT synthesis and purification

BNNTs were synthesized via a metal-catalyst-free, atmospheric pressure induction plasma process (Fig. S1). In this process¹, BNNTs are produced directly from pure hexagonal boron nitride (h-BN) powder (99.5 %, avg. 70 nm, MK-hBN-N70, M K Impex Corp.) by utilizing high-temperature induction thermal plasma (Fig. S1b). Full details on this process and its operating condition can be found elsewhere.¹

From extensive microscopic analysis, BNNTs with an average nanotube diameter of ~5 nm, typically with 2-5 walls, are observed with a uniform distribution of B and N composing the tube walls.¹ Interestingly, raw BNNT materials are produced in semi-assembled forms of fibril, web or aerogel, which can be easily adaptable for fabrication of various macroscopic BNNT assemblies. The main impurities identified in our as-produced material are amorphous boron particles encapsulated with hexagonal boron nitride (h-BN) shells (see Fig. S2), similar to other high-temperature BNNT synthesis routes.²⁻⁴ These are present to a level of 20~30% as estimated from TGA. Purification of the BNNT can greatly reduce the amounts of these impurities.

A scalable, non-destructive post-processing protocol involving a combination of thermal treatments similar to the one reported by Chen et al.,⁵ and solvent washing also has been developed. Figure S3 displays SEM and TEM images, respectively, of a sample processed by our purification protocol. Clean, large-diameter BNNT bundles are observed up to a few hundred nanometers in diameter. Although a small amount of h-BN flakes or shells still exist in the sample (Fig. S3b), the main amorphous B impurity was effectively removed from the sample leaving only hollow h-BN shells (see also TGA data in Fig. S3c). The presence of h-BN shells or flakes should not be critical in many BNNT applications.⁶ Figure S3d shows Raman spectra of the purified sample obtained with two different wavelengths of 514 and 633 nm. The peaks at 1367 or 1369 cm⁻¹ are clearly observed and attributable to the E_{2g} vibration mode of sp² hybridized BN networks.⁷ The small FWHM suggests no significant damage on the walls of BNNTs after purification.

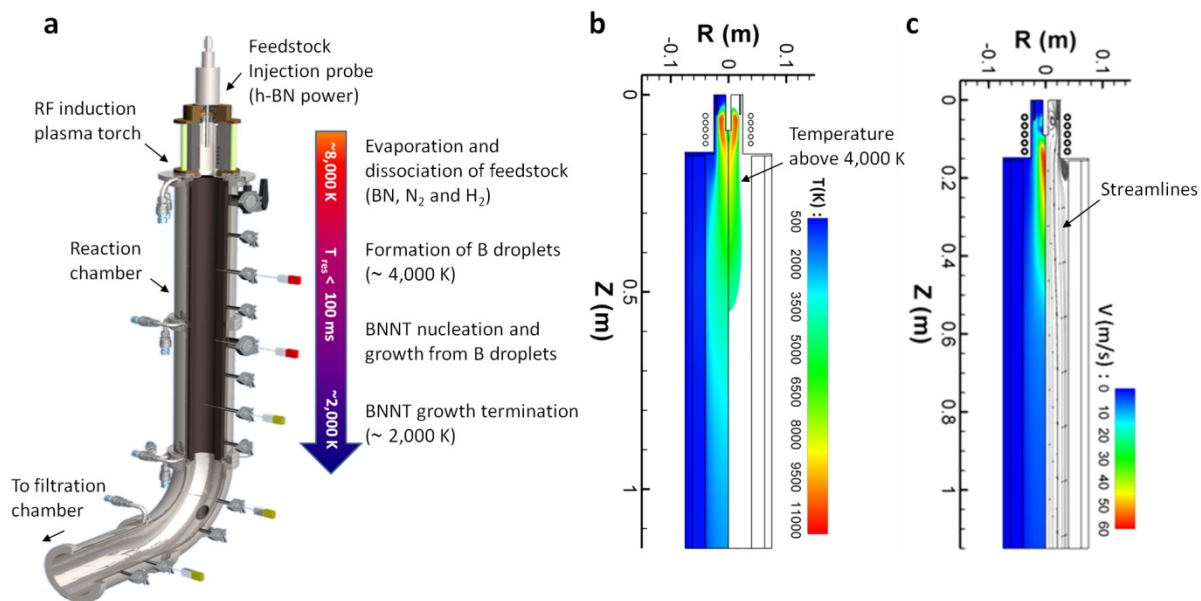


Figure S1. (a) Schematic of an RF induction thermal plasma system developed for the large-scale synthesis of high quality small-diameter BNNTs using the atmospheric pressure HABS process. Pure h-BN powder is continuously transformed into BNNTs by passing through a high temperature N_2 - H_2 plasma (~ 8000 K). (b) Calculated temperature distribution inside the reactor. The right-hand side shows the hot temperature zone above 4000 K. (c) Calculated velocity distribution (left) and streamlines (right). Net plasma power: 35 kW; pressure: 93 kPa; central gas: Ar (30 slpm); sheath gas: a ternary mixture of Ar (45 slpm), N_2 (55 slpm), and H_2 (20 slpm); powder carrier gas: Ar (3 slpm).

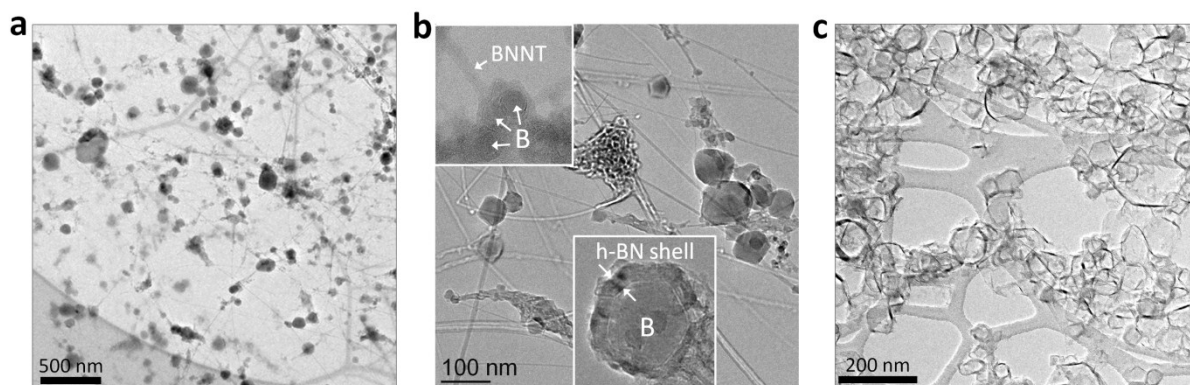


Figure S2. (a) TEM image of the as-produced BNNT material showing the main impurity. Black dots present amorphous B particles. (b) High magnification TEM images of amorphous B particles in the as-produced BNNT sample. Boron particles are encapsulated by h-BN shells. (c) TEM image of a BNNT sample treated with nitric acid (12M HNO_3). Nitric acid leached out amorphous B from h-BN shells but also destroyed BNNTs.

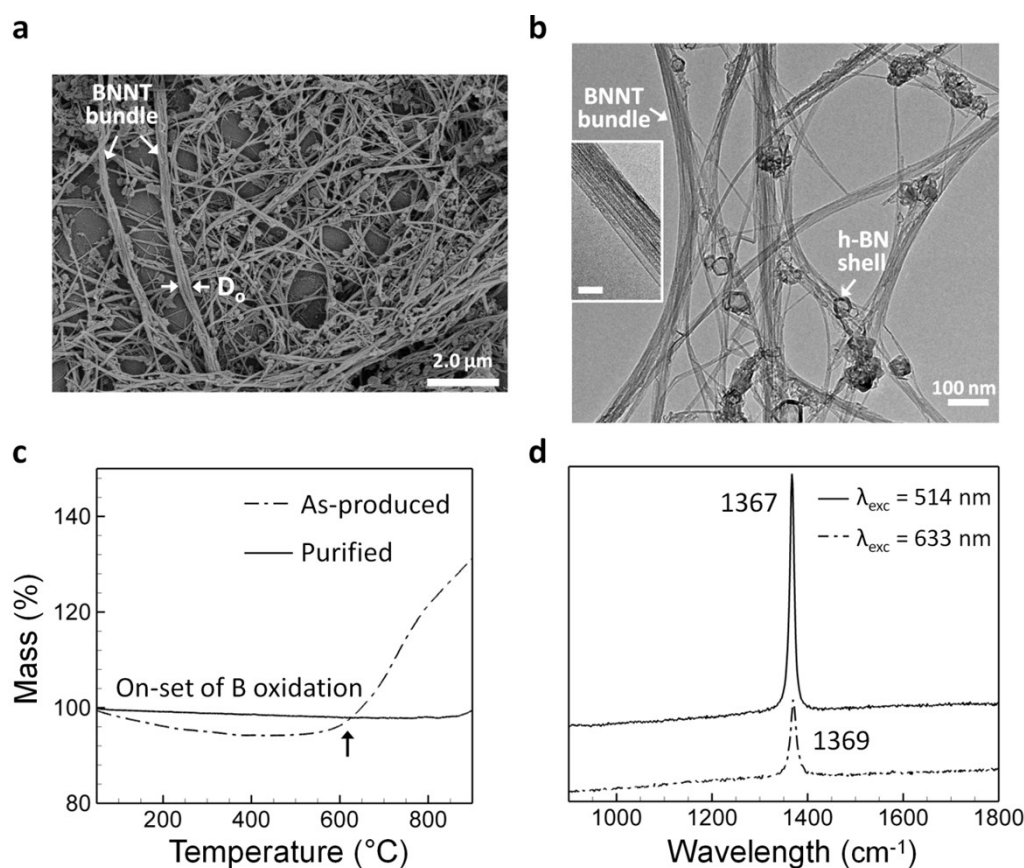


Figure S3. (a) SEM image of a purified BNNT sample. Large BNNT bundles ($D_0 \approx 400$ nm) are easily observed as a result of purification. (b) TEM image of a purified BNNT sample showing that amorphous B particles were effectively removed from h-BN shells without damage on the walls of BNNTs. The scale bar in the inset is 10 nm. (c) TGA data of the as-produced and purified BNNT samples. (d) Raman spectra of a purified BNNT sample measured with two different wavelengths (514 and 633 nm) showing the characteristic BN peak.

Fabrication of BNNT assemblies: BNNT Buckypaper

To fabricate nonwoven sheets composed of nominally 100 % BNNTs, often called buckypapers in the CNT literature, purified BNNTs were dispersed in methanol using shear mixing and bath sonication and then the dispersion was vacuum filtered through a polycarbonate membrane (20 μm pore size, Sterlitech) using a home-built vacuum table that accommodates rectangular funnels up to 30 \times 30 cm in size. The as-filtered buckypaper was sandwiched between sheets of parchment paper and compressed. After partial drying at room temperature under compression, the buckypaper peeled easily from the filtration membrane and was further dried by baking at 100 $^\circ\text{C}$ for 2 h. Using similar techniques, heterobuckypapers composed of both CNTs and BNNTs were prepared through successive filtering of CNT and BNNT solutions. Commercial CNTs (Nanocyl, NC7000) were used.

Characterization

The morphological properties of samples were characterized using a scanning electron microscopy (SEM) (Hitachi, S4700) and a transmission electron microscope (TEM) (FEI Titan cubed 80-300). Thermogravimetric analysis (TGA; Netzsch TG 209 F1 Irish) and Raman spectroscopy (Renishaw inVia Reflex Raman microscope) were employed to analyze the thermal stability and structural properties of BNNT samples, respectively. For the TGA measurements, approximately 10 mg of BNNT material was oxidized in flowing air (50 sccm), using a temperature ramp of 10 °C/min from room temperature to 950 °C.

The mechanical properties of BNNT-polymer nanocomposites were investigated by testing free-standing rectangular specimens under tension until failure. A micro-tensile test frame (Fullam Substage Test Frame) was employed to determine the Young's modulus (E), ultimate tensile strength (UTS) and ultimate tensile strain (ϵ_{max}) of the pristine BNNT buckypapers and the nanocomposite samples. A displacement rate of 1 mm/min was employed. Mechanical properties were also assessed by dynamic mechanical analysis (DMA; TA Instruments Q800) using a tension fixture.

Additional Supplementary Figures

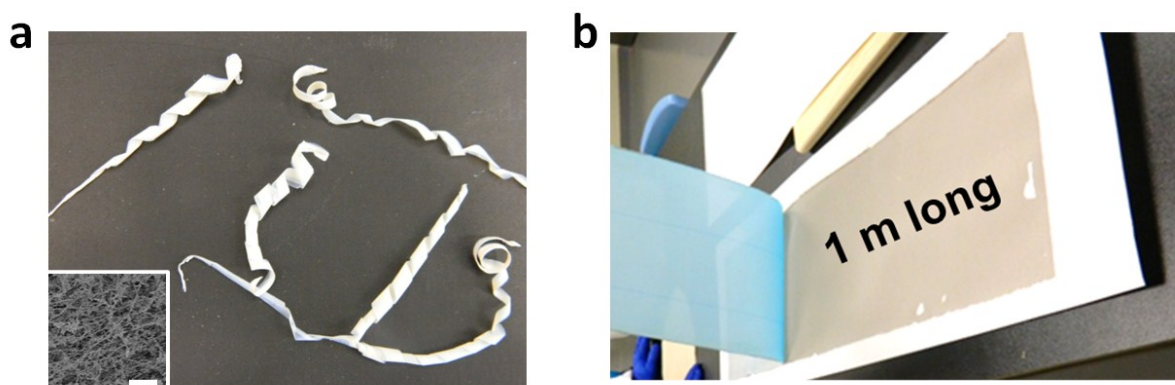


Figure S4. Large-size production of BNNT ribbons and buckypapers. (a) As-produced BNNT ribbons. The inset is a SEM image of a BNNT ribbon and the scale bar is 1 μm . (b) 1meter long buckypaper made from as-produced BNNT materials.

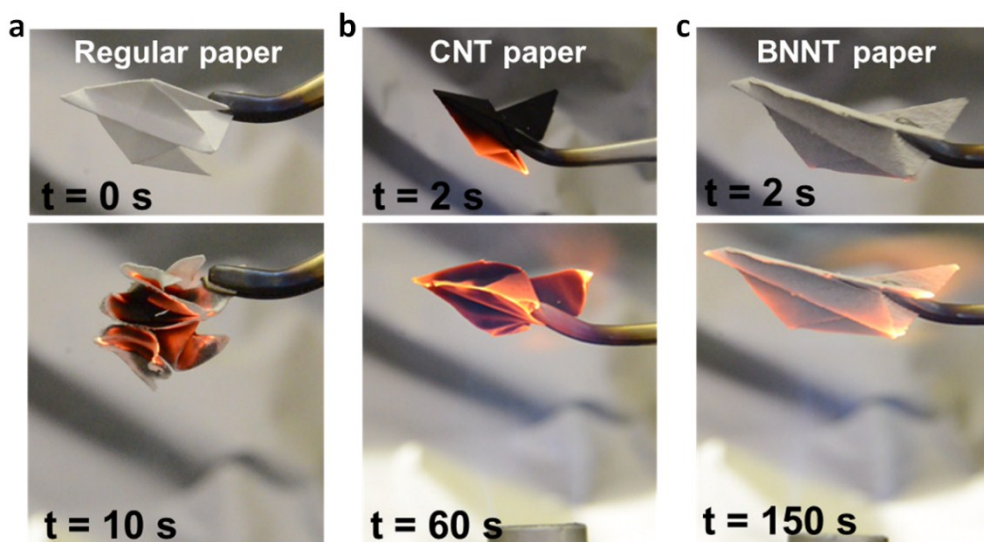


Figure S5. Flame resistance of BNNT paper illustrated by comparison of paper airplanes folded from (a) regular cellulose-based paper, (b) carbon nanotube buckypaper and (c) BNNT buckypaper and exposed to a natural gas flame. The BNNT paper exhibits the highest thermal stability without morphological changes.

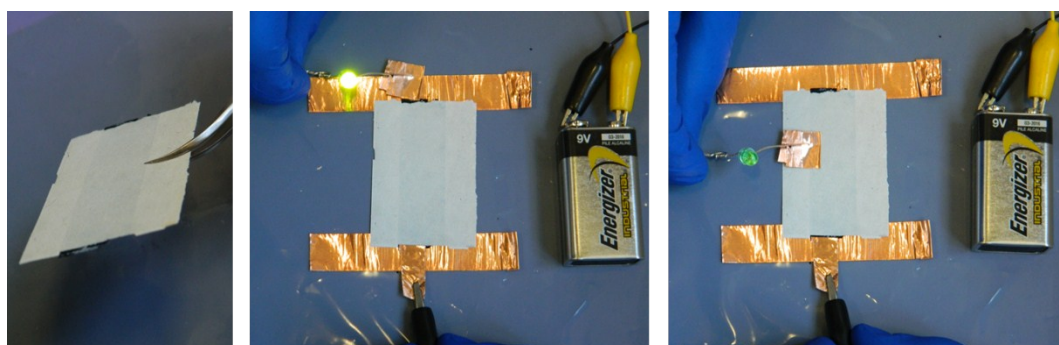


Figure S6. CNT conductors are being developed as lightweight wiring for aerospace and other applications (REF). Here we demonstrate a BNNT-insulated CNT conductor using an MWCNT buckypaper conductor with a BNNT insulator/jacket. A circuit including a green LED is completed, lighting the LED, by contacting the ends of the CNT conductor. The BNNT layer provides high electrical resistance, enabling multi-conductor wires and also offers a solution for a difficult to achieve combination of flexible, high-temperature, flame-resistant wiring.

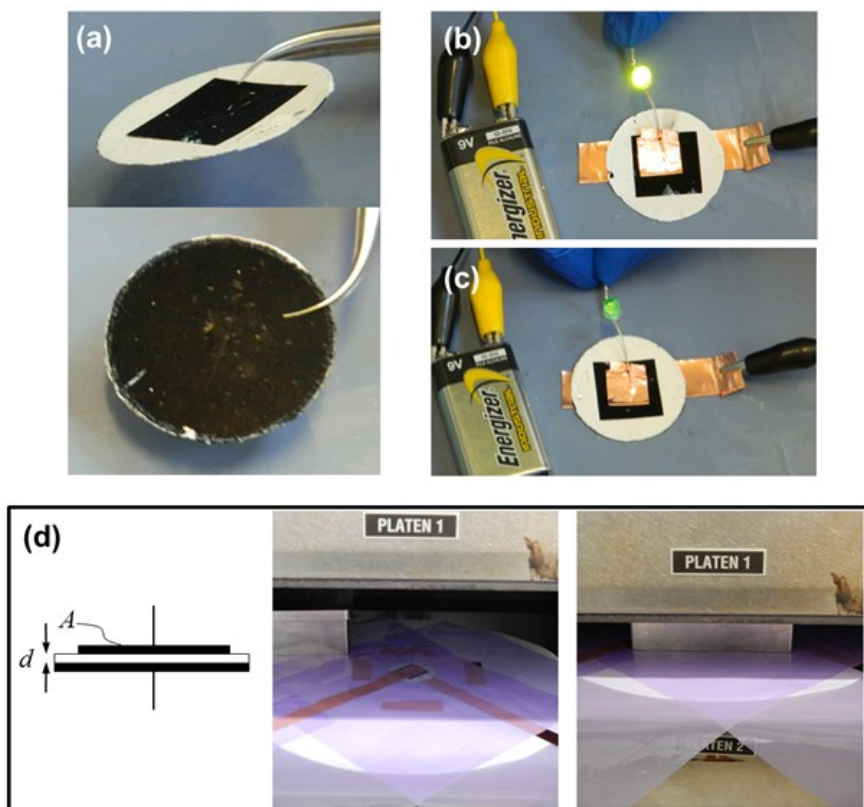


Figure S7. (a) CNT/BNNT/CNT layered buckypaper structures produced either by (1) filtering CNTs, BNNTs and CNTs in sequence, or by (2) exclusively filtering BNNTs through pre-fabricated CNT layers, which requires a post-assembly step. (b) Filtering CNTs through a BNNT layer leads to through-thickness conduction, lighting the LED. (c) If no CNTs are filtered through the BNNT layer the resulting structure is electrically insulating (LED off). (d) Capacitance measurement of this structure using an LCR meter and treating the heterobuckypaper as a parallel plate capacitor indicated an apparent dielectric constant of $k \sim 3$ and no detectable leakage. The photograph shows this measurement performed using copper foil to contact the CNT layers under gentle pressure. As expected, the measured capacitance increased as the assembly was compressed under higher pressure.

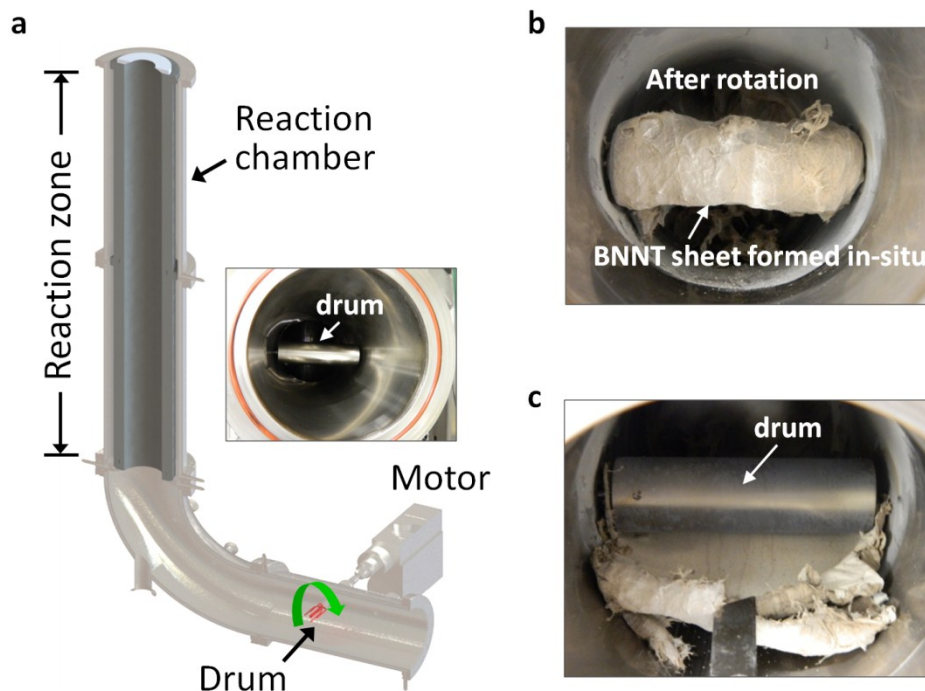


Figure S8. Direct fabrication of BNNT sheets from the synthesis reactor. (a) Schematic drawing of a direct fabrication apparatus. A cylindrical drum used in this work is shown in the inset. (b), (c) Photographs of as-produced BNNT sheet formed in-situ during the BNNT synthesis.

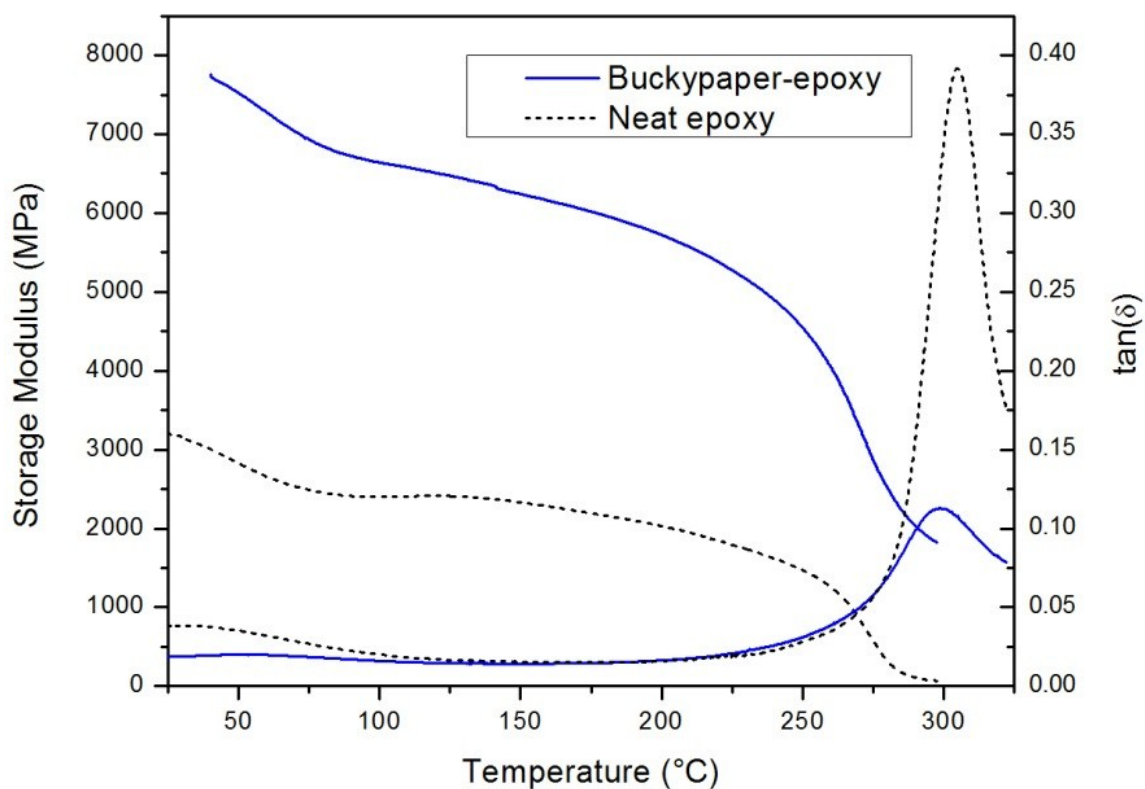


Figure S9. DMA for neat epoxy and epoxy-impregnated BNNT buckypaper.

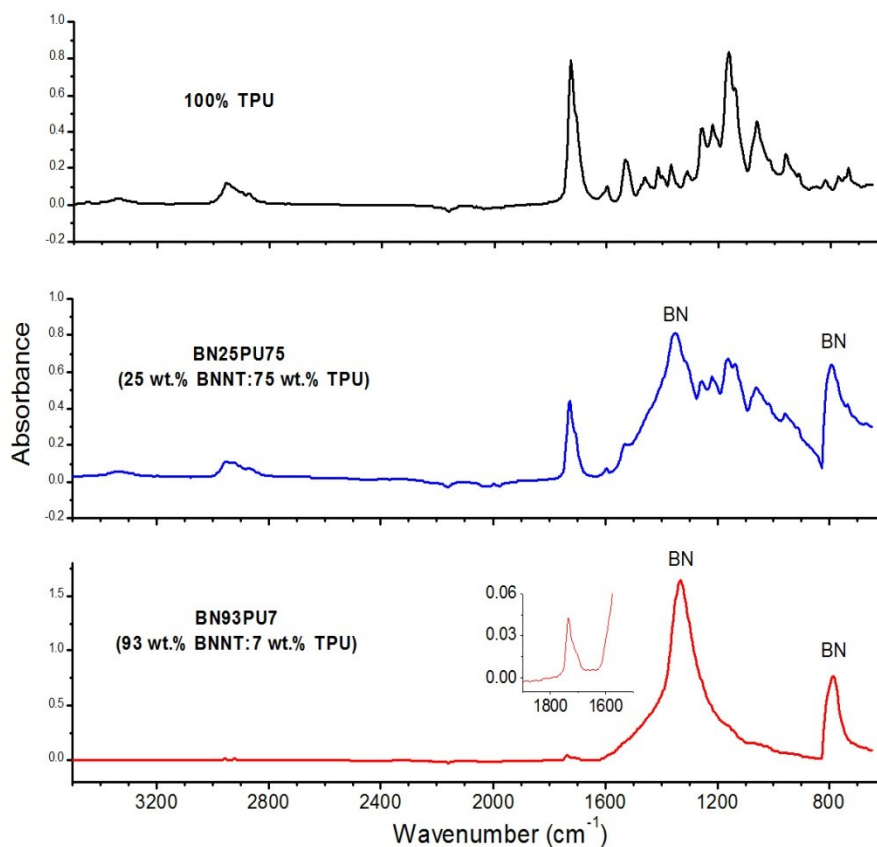


Figure S10. ATR-FTIR spectra for TPU-modified BNNT buckypapers.

References

1. K. S. Kim, C. T. Kingston, A. Hrdina, M. B. Jakubinek, J. Guan, M. Plunkett and B. Simard, *ACS Nano* 2014, **8**, 6211-6220.
2. A. L. Tiano et al., *Biosensors, and Info-Tech Sensors and Systems 2014*, V. K. Varadan (eds), Proc. of SPIE, 2014, 9060, 906006.
3. M. W. Smith, K. C. Jordan, C. Park, J.-W. Kim, P. T. Lillehei, R. Crooks and J. S. Harrison, *Nanotechnology*, 2009, 20, 505604.
4. A. Fathalizadeh, T. Pham, W. Mickelson and A. Zettl, *Nano Lett.*, 2014, 14, 4881-4886.
5. H. Chen, Y. Chen, J. Yu and J. S. Williams, *Chem. Phys. Lett.*, 2006, **425**, 315-319.
6. C. Zhi, Y. Xu, Y. Bando and D. Golberg, *ACS Nano*, 2011, 5, 6571-6577.
7. J. Nemanich, S. A. Solin and R. M. Martin, *Phys. Rev. B*, 1981, 23, 6348-6356.